Mater. Res. Soc. Symp. Proc. Vol. 845 © 2005 Materials Research Society AA4.10

Tissue Engineered Bone Using Polycaprolactone Scaffolds Made by Selective Laser Sintering

J.M. Williams[1], A. Adewunmi[2], R.M. Schek[1,3], C.L. Flanagan[1], P.H. Krebsbach[1,3], S.E. Feinberg[5], S.J. Hollister[1,2,4], S. Das[2]

[1]Biomedical Engineering, [2]Mechanical Engineering, [3]Dentistry, [4]Surgery, [5]Oral and Maxillofacial Surgery, University of Michigan, Ann Arbor, Michigan, 48109-0018, USA

ABSTRACT

Polycaprolactone is a bioresorbable polymer that has potential for tissue engineering of bone and cartilage. In this work, we report on the computational design and freeform fabrication of porous polycaprolactone scaffolds using selective laser sintering, a rapid prototyping technique. The microstructure and mechanical properties of the fabricated scaffolds were assessed and compared to designed porous architectures and computationally predicted properties. Compressive modulus and yield strength were within the lower range of reported properties for human trabecular bone. Finite element analysis showed that mechanical properties of scaffold designs and of fabricated scaffolds can be computationally predicted. Scaffolds were seeded with BMP-7 transduced fibroblasts and implanted subcutaneously in immunocompromised mice. Histological evaluation and micro-computed tomography (μCT) analysis confirmed that bone was generated *in vivo*. Finally, we have demonstrated the clinical application of this technology by producing a prototype mandibular condyle scaffold based on an actual pig condyle.

INTRODUCTION

Repair and reconstruction of complex joints such as the temporo-mandibular joint (TMJ) pose many challenges for bone tissue engineering. Adverse reactions to alloplastic, non-biological materials result in compromised functional outcome in patients and autogenous grafts can lead to complications elsewhere in the patient [1,2]. Tissue engineering may overcome these limitations by the use of scaffolds that fit into anatomic defects, possess mechanical properties that will bear *in vivo* loads, enhance tissue in-growth, and produce biocompatible degradation byproducts [3-9].

Solid freeform fabrication techniques (SFF) enable design and fabrication of anatomically shaped scaffolds with varying internal architectures, thereby allowing precise control over pore size, porosity, permeability, and stiffness [10]. Control over these characteristics may enhance cell infiltration and cellular communications, and mass transport of nutrients and metabolic waste throughout the scaffold. One such SFF method, selective laser sintering (SLS), may be advantageous for creating bone tissue engineering scaffolds for sites such as the TMJ, because it provides a cost-effective, efficient method for constructing scaffolds matching the complex anatomical geometry of craniofacial or periodontal structures, where preformed materials might be difficult or ineffective [1]. SLS constructs scaffolds from 3-D digital data by sequentially fusing selected regions in a powder bed, layer by layer, via a computer controlled scanning laser beam [11,12]. With SLS, virtually any powdered biomaterial that will fuse but not decompose under a laser beam can be used to fabricate scaffolds with complex internal and external geometries. Thus, SLS has strong potential for fabricating tissue engineering scaffolds [13-21].

Polycaprolactone (PCL) is a bioresorbable polymer that has potential for tissue engineering of bone and cartilage. Scaffolds have previously been created in PCL with a variety of SFF techniques including fused deposition modeling [22-30], photopolymerization of a synthesized PCL macromer [31], shape deposition manufacturing [32], precision extruding deposition [33], three dimensional printing [34], low temperature deposition [35] and multi-nozzle freeform deposition [33,36-41]. However, the fabrication and characterization of PCL scaffolds with varying internal architectures and porosities made by SLS has not been reported.

We propose to use PCL scaffolds fabricated using SLS to engineer bone tissue. For successful utilization of PCL scaffolds in bone tissue engineering, their construction from computational designs must be anatomically accurate, their mechanical properties should lie within an appropriate physiological range, and they must support the in-growth of bone tissue. Towards this end, we manufactured scaffolds in a variety of designs. We evaluated the microstructure using micro-computed tomography (μCT), and mechanical properties using compression testing and finite element analysis (FEA). We evaluated the biological properties of these scaffolds by seeding them with bone morphogenetic protein-7 (BMP-7) transduced human fibroblasts and evaluated the generated tissue using μCT and histology. Finally, to demonstrate the clinical potential of this technology, we employed image-based design techniques to superimpose computed tomography (CT) data with a designed porous architecture to build a complex scaffold that mimics a mandibular condyle. Results show that manufactured scaffolds matched the designs well, had compressive strength and modulus values within the range of trabecular bone, and supported the in-growth of bone in an *in vivo* model. The work presented here is the one of the first reported efforts on the design, manufacture and, mechanical and biological characterization of PCL scaffolds built by SLS.

MATERIALS AND METHODS

Porous scaffold design and fabrication

Cylindrical porous scaffolds (12.7 mm diameter, 25.4 mm height), with three-dimensional orthogonal periodic porous architectures, were designed using Unigraphics NX 3-D solid modeling software (UGS PLM Solutions, Plano, TX). The designs were then exported to a Sinterstation 2000™ SLS machine (3D Systems, Valencia, CA) in STL file format, and were used to construct scaffolds by SLS processing of ε-polycaprolactone powder (CAPA 6501, Solvay Caprolactones, Warrington, Cheshire, UK). This particular form of PCL has a melting point of 60°C, a molecular weight of 50,000 Da, and 10-100 μm particle size distribution. SLS processing of the PCL powder was conducted by preheating the powder to 49.5°C and scanning the laser (450μm focused beam diameter) at 4.5 Watts power and 1.257 m/s (49.5 inches/s) scan speed, and by using 100μm.thick powder layers.

Six different periodic orthogonal pore architecture designs were created and 7 specimens for each design were manufactured for microstructure analysis and mechanical testing. The pores ranged from 1.75-2.5 mm in diameter, producing scaffolds with 63-79% designed volumetric porosity as calculated from the STL files (see Table 1). Seven solid cylindrical specimens were also created to determine the bulk properties obtainable by SLS. Six cylindrical porous scaffolds (5.0 mm diameter, 4.5 mm height, 1.5mm diameter orthogonal interconnected pores, porosity=68%) were designed and manufactured for *in vivo* testing.

Microstructural Analysis, Mechanical Property Measurements and Image-Based FEA

Two specimens from each experimental group (n=7) were scanned in air using a MS-130 high resolution μCT scanner (GE Medical Systems, Toronto, CAN) at 28 μm voxel resolution, at 75 kV and 75 mA. The porosity of each specimen was calculated by defining a region of interest and an appropriate threshold level to delineate the solid PCL material using GEMS Microview software (GE Medical Systems, Toronto, CAN).

Seven specimens from each experimental group, including the two that were used for microstructure analysis, were mechanically tested in compression in accordance with ASTM D695-02a using an MTS Alliance RT30 test frame (MTS Systems Corp., MN).

Effective stiffness constants were calculated using the voxel-based homogenization finite element analysis (FEA) software VOXELCON (Quint Corp, Tokyo, Japan). Voxel models were created of both the design STL files and the corresponding voxelized μCT scans for each scaffold design built by SLS. For FEA, PCL material properties were assumed isotropic with 120 MPa Young's modulus (bulk property of PCL processed by SLS) and Poisson's ratio of 0.3.

Cell seeding and implantation

Primary human gingival fibroblasts (HGF) were prepared from explants of human surgical waste in compliance with the University of Michigan Institutional Review Board [1]. Passage 4 fibroblasts were infected with AdCMV-BMP-7, a recombinant adenovirus construct expressing the murine BMP-7 gene under a cytomegalovirus (CMV) promoter [42]. Such infected primary cells have been shown to form bone *in vivo* [43-49]. Two million cells were seeded into each scaffold by suspending them in 30 μl of 2 mg/ml collagen gel made from acid-solubilized rat tail collagen (BD Biosciences, Bedford, MA), which was gelled using 37°C incubation [50]. Six scaffolds were then implanted in 5 to 8 week old immunocompromised mice (N:NIH-bg-nu-xid, Charles River, Wilmington, MA). Animals were anesthetized with injections of ketamine/xylazine (50 μg/g and 5 μg/g, respectively), subcutaneous pockets were created, four scaffolds were inserted into each mouse and surgical sites were closed with wound clips.

The animals were sacrificed at 4 weeks after implantation. The harvested implants were fixed using Z-Fix (Anatech, Battle Creek, MI) and stored in 70% ethanol for μCT analysis. Specimens were scanned in water using a MS-130 high resolution μCT scanner at 16 μm voxel resolution, at 75 kV and 75 μA. Three-dimensional isosurface renderings of the mineralized tissue were made using MicroView to visualize the remaining scaffold and the generated tissue. The reconstructed 3D data sets were used to calculate the volume of bone present on the scaffolds and the average density of the new bone using MicroView's automated image analysis and thresholding features. Following μCT scanning, the scaffolds were demineralized using RDO (APEX Engineering Products Corp, Plainfield, IL). The scaffolds were then embedded in paraffin, sectioned at 7 μm, and stained with hematoxylin and eosin (H&E).

Mandibular condyle design and fabrication

To demonstrate proof of concept, a minipig mandibular condyle scaffold was designed using image-based techniques [51]. A global anatomic design was first created directly from the CT scan of a minipig mandible. A ramus attachment collar was then digitally added using specially written software. The scaffold microstructure, consisting of interconnected cylindrical

pores, was also created using specially written image-based design software [52]. The global anatomic condyle design was then combined with the scaffold architecture design using Boolean operations. The final result (Figure 9b) was a porous, anatomically shaped mandibular condyle scaffold that can be attached to the mandibular ramus via the designed collar.

RESULTS AND DISCUSSION

Microstructure analysis

A representative image of the STL file (Figure 1a) used to manufacture a scaffold, and the corresponding porous cylindrical scaffold built by SLS (Figure 1b) illustrates our ability to manufacture designed scaffolds. Porous PCL scaffolds with six different internal pore architectures and 63-79% design porosities (Table 1) were designed and fabricated. Their porosities were computed by μCT analysis (Figure 2b). The designed and actual scaffold porosities were well correlated and directly related with a slope of nearly 1 (Figure 2c). However, the least squares regression fit does not pass through the origin, illustrating that the manufactured porosity is consistently 27% less than the design porosity for the porous scaffolds (Table 1). The solid cylindrical scaffold had 0% design porosity and 17.8% actual porosity.

Experimental mechanical property assessment

Proper assessment of the mechanical properties of PCL scaffolds fabricated through SLS is necessary to ensure that the scaffold properties are within the range of human trabecular bone. Scaffold mechanical properties matching those of trabecular bone are important for early functional loading, which could also be beneficial to enhance bone formation and in-growth [25]. Compressive modulus values of human trabecular bone range from 1-5000 MPa, with strength values ranging from 0.10-27.3 MPa [6,9,53-61] with mean values of approximately 194 MPa and 3.55MPa, respectively [62]. The mechanical properties of the PCL scaffolds are reported in Table 1 where "experimental" values are from compression testing and "computational" results are produced by finite element analysis on the design files (for design parameters) or on μCT images of the scaffolds (for actual scaffolds). Mean experimental and computational compressive modulus values for the porous scaffolds fell within the lower range of human trabecular bone [62], varying from 52-67 MPa and 46-68 MPa respectively (Table 1). Mean experimental yield strength data also fell within the lower range of human trabecular bone [62], varying from 2.0-3.2 MPa (Table 1). In order to verify that the bulk material properties for compressive modulus of PCL were consistent with the value of 120MPa reported by Solvay, SLS processed solid PCL cylinders were mechanically tested in compression. Experimental data confirmed that the compressive modulus of the bulk PCL material was approximately 120 MPa. The strength and modulus for each scaffold were plotted against volume fraction for the purpose of relating compressive mechanical properties to volume fraction (Figure 3). Both compressive modulus and compressive yield strength showed positive correlations with volume fraction, with R^2 values of 0.4634 and 0.7938, respectively.

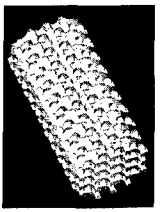

Figure 1. (a) STL design file for the 1.75mm x/y/z porous scaffold.

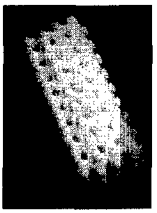

Figure 1. (b) PCL scaffold fabricated by SLS.

Table 1. Scaffold design parameters, design porosities and compressive mechanical properties.

Design Parameters		Design Scaffolds					
		Porosity	Computational	Porosity (μ-CT)			
		(%)	E (Mpa)	(%)			
1.75	1.75	63.1	22.5	37.5±1.5	65±3	3.2±0.5	57±7
2	2	69.3	17.2	46.2±0.2	52±2	2.2±0.1	53±3
1.75	2	69.2	21.1	41.7±0.8	63±4	2.8±0.1	68±4
1.75	2.25	74.5	20.7	45.5±0.1	67±4	2.9±0.2	62±8
2	2.25	74.2	17.3	50.2±0.1	55±3	2.3±0.1	48±1
2	2.5	79.0	16.1	55±0.9	54±3	2.0±0.1	46±3
Solid		0.0	120.0	17.8±0.7	122±13	11.7±0.5	112±12

Computational compressive modulus (E) was calculated for each scaffold design by performing FEA on each design's STL file. Actual scaffold porosities and mechanical properties of the seven different scaffold architectures are also shown. Experimental modulus and yield strength values were calculated through unconfined compression testing. Computational modulus values were calculated by performing FEA on μCT scans of the scaffolds.

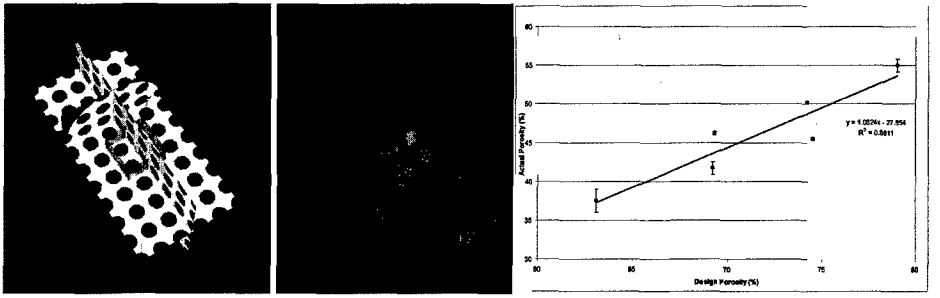

(a) (b) (c)

Figure 2. (a) A voxel rendering of the scaffold's STL file used to perform FEA on the designed architecture. (b) A voxel rendering of the scaffold's μCT structure used for volume fraction calculations and for performing FEA on the actual scaffold. (c) Correlation between targeted scaffold design porosities and actual scaffold porosities measured by μCT. A least squares regression line is fit to the data to show correlation.

Image based FEA

Compressive moduli computed by FEA on the design STL files correlated well with the experimentally measured moduli (Figure 4a), but were approximately half the experimental moduli. Image-based finite element (FE) models created directly from μCT scans of fabricated scaffolds did account for the increased volume fraction in the actual scaffold over the design, and thus verified the ability of image-based FE models to compute scaffold stiffness prior to implantation without the need for destructive testing. Testing the actual PCL scaffolds both

experimentally and computationally validated the computationally predicted data relative to the experimental data for compressive modulus, as illustrated by the correlation in Figure 4b.

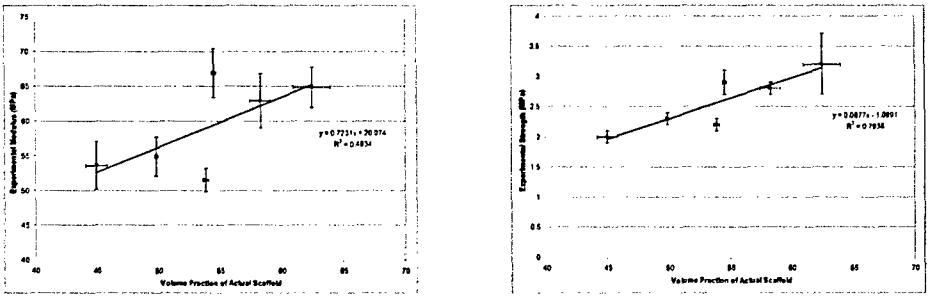

(a) (b)

Figure 3. Differences in correlation within (a) experimental modulus and volume fraction and (b) experimental yield strength and volume fraction is likely due to varying design geometries.

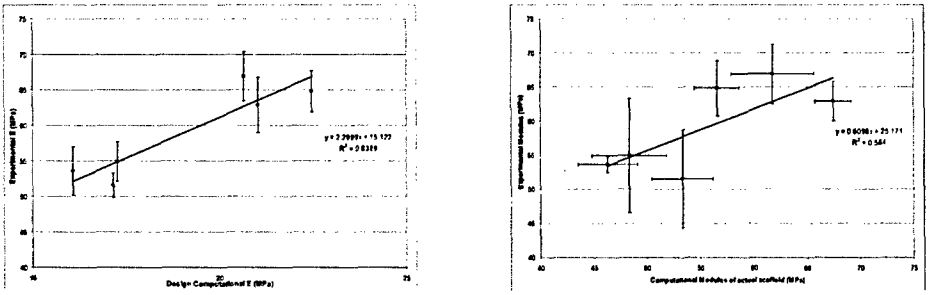

(a) (b)

Figure 4. (a) Close correlation exists between the computational E value of each design file, and the experimental E value of the corresponding fabricated (actual) scaffolds. (b) Correlation between computational modulus of fabricated scaffolds and experimental modulus of fabricated (actual) scaffolds.

Generation of Bone *In Vivo*

Micro-CT data indicated that 5.02 (+/-2.2) mm^3 of bone formed on or inside the orthogonal pore scaffolds (initial scaffold volume = 99.5 mm^3). The volumetric bone mineral density (BMD) measures of the newly formed bone inside the scaffold pores or on the scaffold surfaces was 513.36 (+/-14.23) mg/cm^3. The BMD of the newly formed bone lies within the range of normal BMD measures of human trabecular and cortical bone, 120 mg/cm^3 and 1100 mg/cm^3, respectively [63]. Micro-CT images and bone surface renderings shown in Figures 5 and 6a illustrate the newly formed bone that has grown onto and within a representative orthogonal pore scaffold after 4 weeks of implantation. Histological staining confirmed the presence of bone reported by μCT. Figure 6b shows a cortex surrounding the implant. Figure 6c reveals the presence of normal bone morphology, including osteocytes, trabeculated structures, and marrow space. Large amounts of bone are shown around the exterior of the scaffold, as well as within

the scaffold pores. Both μCT and histological staining reveal the presence of a cortex that enveloped around the entire implant, and is similar to results obtained using other materials [64]. Inside the "shell", marrow space and trabecular bone was observed both on the scaffold exterior and penetrating into the scaffold pores (Figure 6).

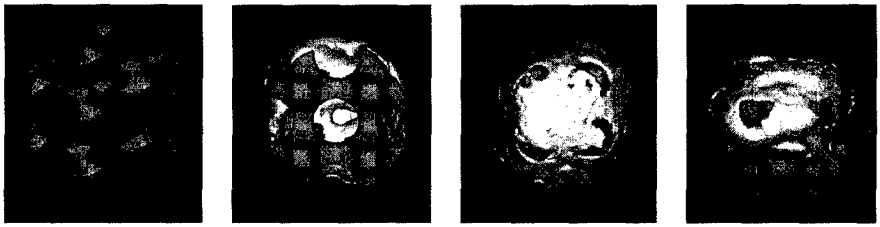

(a) (b) (c) (d)

Figure 5. (a) Isometric view the STL design file for the subcutaneous-size scaffold, (b) bottom view, (c) top view, (d) side view of μCT bone surface rendering data combined with the STL design file. PCL scaffold is shown in blue and bone is shown in white.

(a) (b) (c)

Figure 6. (a) Top view of actual μCT data slice image (same orientation as 5c) shows cortical shell and areas of trabeculated structures within the marrow space that correspond to histological staining (H&E) shown in (b) and (c).

Mandibular Condyle Design and Fabrication

The SLS technique successfully built mandibular condyle (Figure 7a) scaffolds designed using image-based design techniques (Figure 7b) in approximately 3 hours (Figures 7c & 7d).

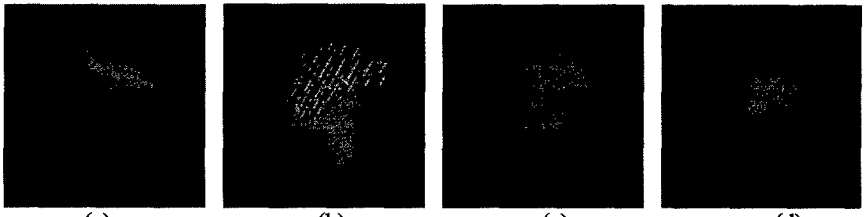

(a) (b) (c) (d)

Figure 7. (a) An actual pig condyle, (b) surface rendering of STL design file for pig condyle scaffold, (c) front view, and (d) back view of pig condyle PCL scaffold fabricated by SLS.

CONCLUSIONS

PCL scaffolds fabricated via SLS show great potential for replacement of skeletal tissues. The results indicate that SLS fabricated PCL scaffolds can satisfy the requirements for bone tissue engineering. These scaffolds possess mechanical properties within the lower range of trabecular bone, suggesting they may have the ability to withstand early functional loading. The success in manufacturing the designed scaffolds, achieving appropriate mechanical characteristics, and their ability to support the in-growth of bone show their potential for use in tissue engineering. We have also shown that computational analysis of these scaffolds can provide assessment of their mechanical properties without the need for destructive testing. By successfully fabricating a mandibular condyle scaffold implant, we have demonstrated a method combining image-based computational design and SFF for producing biomimetic bone tissue engineering scaffolds in PCL. We have shown that scaffolds with both intricate external geometry and controlled internal architecture can be produced by SLS of PCL. Such scaffolds can be easily manufactured to fit complex anatomic locations, demonstrated by, but not anatomically limited to, fabrication of a mandibular condyle. The fabrication of PCL scaffolds via a combination of computationally optimized, patient specific digital designs and SLS may ultimately result in a viable technique for the repair and regeneration of bone and cartilage in the future.

ACKNOWLEDGEMENTS

This research was supported by NIH grants DE 13608 (Bioengineering Research Partnership) and R21 DE 014736.

REFERENCES

1. R.B. Rutherford, K. Gu, P. Racenis, and P.H. Krebsbach, Connect Tissue Res, **44** (1), Suppl 1:117-123 (2003)
2. L.G. Mercuri, Oral Surg Oral Med Oral Pathol Oral Radiol Endod, **85** (6), 631-7 (98)
3. S. Das and S.J. Hollister, Encyclopedia of Materials: Science and Technology, 2003)
4. C.M. Agrawal and R.B. Ray, J. Biomed Mater Res, **55** (2), 141-150 (2001)
5. L. Griffith, Acta mater., **48** (263-277 (2000)
6. R. Langer and D.A. Tirrell, Nature, **428** (6982), 487-92 (2004)
7. C.M. Agrawal and R.B. Ray, J. Biomed Mater Res, **55** (2), 141-150 (2001)
8. L. Griffith, Acta mater., **48** (263-277 (2000)
9. R. Langer and D.A. Tirrell, Nature, **428** (6982), 487-92 (2004)
10. R. Landers, A. Pfister, U. Hubner, H. John, R. Schmelzeisen, and R. Mulhaupt, Journal of Materials Science, **37** (15), 3107-3116 (2002)
11. C.R. Deckard, M.S. Thesis, University of Texas at Austin, 1986.
12. C.R. Deckard, Ph.D. Thesis, University of Texas at Austin, 1988.
13. N.K. Vail, L.D. Swain, W.C. Fox, T.B. Aufdlemorte, G. Lee, and J.W. Barlow, Materials & Design, **20** (2-3), 123-132 (99)
14. K.H. Tan, C.K. Chua, K.F. Leong, C.M. Cheah, P. Cheang, M.S. Abu Bakar, and S.W. Cha, Biomaterials, **24** (18), 3115-3123 (2003)
15. I.V. Shishkovsky, E.Yu. Tarasova, L.V. L. V. Zhuravel, and A.L. Petrov, Technical Phys Lett, **27** (3), 211-213 (2001)
16. E. Berry, J.M. Brown, M. Connell, C.M. Craven, N.D. Efford, A. Radjenovic, and M.A.

Smith, Med Eng Phys, **19** (1), 90-96 (97)
17. S. Das, S.J. Hollister, C. Flanagan, A. Adewunmi, K. Bark, C. Chen, K. Ramaswamy, D. Rose, and E. Widjaja, Rapid Prototyping Journal, **9** (1), 43-49 (2003)
18. N.K. Vail, L.D. Swain, W.C. Fox, T.B. Aufdlemorte, G. Lee, and J.W. Barlow, Materials & Design, **20** (2-3), 123-132 (99)
19. I.V. Shishkovsky, E.Yu. Tarasova, L.V. L. V. Zhuravel, and A.L. Petrov, Technical Phys Lett, **27** (3), 211-213 (2001)
20. K.H. Tan, C.K. Chua, K.F. Leong, C.M. Cheah, P. Cheang, M.S. Abu Bakar, and S.W. Cha, Biomaterials, **24** (18), 3115-3123 (2003)
21. S. Das, S.J. Hollister, C. Flanagan, A. Adewunmi, K. Bark, C. Chen, K. Ramaswamy, D. Rose, and E. Widjaja, Rapid Prototyping Journal, **9** (1), 43-49 (2003)
22. I. Zein, D.W. Hutmacher, K.C. Tan, and S.H. Teoh, Biomaterials, **23** (4), 1169-1185 (2002)
23. D. Rohner, D.W. Hutmacher, T.K. Cheng, M. Oberholzer, and B. Hammer, J Biomed Mater Res Part B: Appl Biomater, **66B** (574-580 (2003)
24. D.W. Hutmacher, J. Biomater Sci Polymer Edn, **12** (1), 107-124 (2001)
25. D.W. Hutmacher, Biomaterials, **21** (24), 2529-2543 (2000)
26. D.W. Hutmacher, T. Schantz, I. Zein, K.W. Ng, S.H. Teoh, and K.C. Tan, J. Biomed Mater Res, **55** (2), 203-216 (2001)
27. D.W. Hutmacher, Biomaterials, **21** (24), 2529-2543 (2000)
28. D.W. Hutmacher, T. Schantz, I. Zein, K.W. Ng, S.H. Teoh, and K.C. Tan, J. Biomed Mater Res, **55** (2), 203-216 (2001)
29. D. Rohner, D.W. Hutmacher, T.K. Cheng, M. Oberholzer, and B. Hammer, J Biomed Mater Res Part B: Appl Biomater, **66B** (574-580 (2003)
30. I. Zein, D.W. Hutmacher, K.C. Tan, and S.H. Teoh, Biomaterials, **23** (4), 1169-1185 (2002)
31. H. Kweon, M.K. Yoo, I.K. Park, T.H. Kim, H.C. Lee, H.-S. Lee , J.-S. Oh, T. Akaike, and C.-S. Cho, Biomaterials, **24** (5), 801-808 (2003)
32. K.G. Marra, J.W. Szem, P.N. Kumta, P.A. DiMilla, and L.E. Weiss, J Biomed Mater Res, **47** (3), 324-335 (99)
33. F. Wang, L. Shor, A. Darling, W. Sun, S. Guceri, and A. Lau, 2003)
34. B.M. Wu, S.W. Borland, R.A. Giordano, L.G. Cima, E.M. Sachs, and M.J. Cima, J Controlled Release, **40** (1-2), 77-87 (96)
35. Z. Xiong, Y. Yan, S. Wang, R. Zhang, and C. Zhang, Scripta Materialia, **46** (11), 771-776 (2002)
36. W. Sun, B. Starly, A. Darling, and C. Gomez, J. Biotech Appl Biochem, **39** (1), 49-58 (2004)
37. W. Sun, A. Darling, B. Starly, and J. Nam, J. Biotech Appl Biochem, **39** (1), 29-47 (2004)
38. W. Sun and P. Lal, Comp Meth Prog Biomed, **67** (85-103 (2002)
39. W. Sun and P. Lal, Comp Meth Prog Biomed, **67** (85-103 (2002)
40. W. Sun, B. Starly, A. Darling, and C. Gomez, J. Biotech Appl Biochem, **39** (1), 49-58 (2004)
41. F. Wang, L. Shor, A. Darling, W. Sun, S. Guceri, and A. Lau, 2003)
42. R.T. Franceschi, D. Wang, P.H. Krebsbach, and R.B. Rutherford, J Cell Biochem, **78** (3), 476-86 (2000)
43. D. Gazit, G. Turgeman, P. Kelley, E. Wang, M. Jalenak, Y. Zilberman, and I. Moutsatsos, J

Gene Med, **1** (2), 121-33 (99)
44. P.H. Krebsbach, K. Gu, R.T. Franceschi, and R.B. Rutherford, Hum Gene Ther, **11** (8), 1201-10 (20)
45. R.B. Rutherford, M. Moalli, R.T. Franceschi, D. Wang, K. Gu, and P.H. Krebsbach, Tissue Eng, **8** (3), 441-52 (2002)
46. J.R. Lieberman, L.Q. Le, L. Wu, G.A. Finerman, A. Berk, O.N. Witte, and S. Stevenson, J Orthop Res, **16** (3), 330-9 (98)
47. J.R. Lieberman, L.Q. Le, L. Wu, G.A. Finerman, A. Berk, O.N. Witte, and S. Stevenson, J Orthop Res, **16** (3), 330-9 (98)
48. R.B. Rutherford, M. Moalli, R.T. Franceschi, D. Wang, K. Gu, and P.H. Krebsbach, Tissue Eng, **8** (3), 441-52 (2002)
49. P.H. Krebsbach, K. Gu, R.T. Franceschi, and R.B. Rutherford, Hum Gene Ther, **11** (8), 1201-10 (20)
50. R.M. Schek, S.J. Hollister, and P.H. Krebsbach, Mol Ther, **9** (1), 130-8 (2004)
51. S.J. Hollister, R.A. Levy, T.M. Chu, J.W. Halloran, and S.E. Feinberg, Int J Oral Maxillofac Surg, **29** (1), 67-71 (2000)
52. S.J. Hollister, R.D. Maddox, and J.M. Taboas, Biomaterials, **23** (20), 4095-103 (2002)
53. B.D. Porter, J.B. Oldham, S.L. He, M.E. Zobitz, R.G. Payne, K.N. An, B.L. Currier, A.G. Mikos, and Y. MJ, J Biomech Eng, **122** (3), 286-288 (2000)
54. J. Ouyang, G.T. Yang, W.Z. Wu, Q.A. Zhu, and S.Z. Zhong, Clinical Biomechanics, **12** (7/8), 522-524 (97)
55. S.M. Lang, D.D. Moyle, E.W. Berg, N. Detorie, A.T. Gilpin, N.J. Pappas Jr, J.C. Reynolds, M. Tkacik, and R.L. Waldron 2nd, J Bone Joint Surg Am, **70** (10), 1531-8 (88)
56. 88-89 (97)
57. J.C. Lotz, T.N. Gerhart, and W.C. Hayes, J Comput Assist Tomogr, **14** (1), 107-14 (90)
58. J. Ouyang, G.T. Yang, W.Z. Wu, Q.A. Zhu, and S.Z. Zhong, Clinical Biomechanics, **12** (7/8), 522-524 (97)
59. 88-89 (97)
60. B.D. Porter, J.B. Oldham, S.L. He, M.E. Zobitz, R.G. Payne, K.N. An, B.L. Currier, A.G. Mikos, and Y. MJ, J Biomech Eng, **122** (3), 286-288 (2000)
61. J.C. Lotz, T.N. Gerhart, and W.C. Hayes, J Comput Assist Tomogr, **14** (1), 107-14 (90)
62. R.W. Goulet, S.A. Goldstein, M.J. Ciarelli, J.L. Kuhn, M.B. Brown, and L.A. Feldkamp, J Biomechanics, **27** (4), 375-389 (94)
63. Q. Chen, H. Kaji, M.F. Iu, R. Nomura, H. Sowa, M. Yamauchi, T. Tsukamoto, T. Sugimoto, and K. Chihara, J Clin Endocrinol Metab, **88** (10), 4655-8 (2003)
64. R.M. Schek, J. Mazumder, S.J. Holliser, and P.H. Krebsbach, 50th Annual Meeting of the Orthopaedic Reseach Society, **Poster No: 0743** (2004)